Structure of GeO_2–P_2O_5 glasses studied by x-ray and neutron diffraction

2006 J. Phys.: Condens. Matter 18 1847

(http://iopscience.iop.org/0953-8984/18/6/002)

INSTITUTE OF PHYSICS PUBLISHING JOURNAL OF PHYSICS: CONDENSED MATTER

J. Phys.: Condens. Matter **18** (2006) 1847–1860 doi:10.1088/0953-8984/18/6/002

Structure of GeO_2–P_2O_5 glasses studied by x-ray and neutron diffraction

U Hoppe[1], R K Brow[2], B C Tischendorf[2], P Jóvári[3,4] and A C Hannon[5]

[1] Institut für Physik, Universität Rostock, Rostock D-18051, Germany
[2] Graduate Center for Materials Research, University of Missouri-Rolla, Rolla, MO 65409, USA
[3] Hamburger Synchrotronstrahlungslabor (HASYLAB) am Deutschen Elektronen-Synchrotron (DESY), Notkestraße 85, Hamburg D-22607, Germany
[4] Research Institute for Solid State Physics and Optics, Hungarian Academy of Sciences, POB 49, Budapest H-1525, Hungary
[5] ISIS Facility, Rutherford Appleton Laboratory, Chilton, Didcot OX11 0QX, UK

Received 15 November 2005, in final form 3 January 2006
Published 23 January 2006
Online at stacks.iop.org/JPhysCM/18/1847

Abstract

The structures of three $x GeO_2$–$(1-x)P_2O_5$ glasses, where $x = 0.98$, 0.88, and 0.81, have been studied by neutron and x-ray diffraction experiments that yield well resolved P–O and Ge–O bond distances. The Ge–O coordination number (N_{GeO}) increased from 4.0 ± 0.2 to 4.5 ± 0.2 with the decrease in x from 0.98 to 0.81. The increase in N_{GeO} is consistent with a structural model that assumes that all oxygen form Ge–O–Ge and P–O–Ge linkages between Ge polyhedra and P tetrahedra and that new GeO_5 or GeO_6 polyhedra are formed with isolated PO_4 units when P_2O_5 is added to GeO_2. The bond valencies in the P–O bonds of the PO_4 tetrahedra are greater than unity and are balanced in P–O–Ge bridges with underbonded Ge–O links in the GeO_5 or GeO_6 polyhedra. Mixed site connections are expected for the GeO_5 (or GeO_6) and PO_4 units in glasses with relatively low (<20 mol%) P_2O_5 content due to the overwhelming fraction of GeO_4 tetrahedra. The structural changes are compared with those reported for alkali germanate glasses. Several features indicate different characteristics for the compositional dependence of N_{GeO} for the GeO_2–P_2O_5 and alkali germanate glasses. However, the distributions of the first-neighbour Ge–O distances are found to be nearly identical for the GeO_2–P_2O_5 and K_2O–GeO_2 glasses of equimolar K_2O and P_2O_5 content.

1. Introduction

The compositional dependence of the molar volume and the refractivity of GeO_2–P_2O_5 glasses indicates that the average oxygen coordination number (N_{GeO}) of Ge atoms increases with increasing P_2O_5 content [1]. This phenomenon is similar to that found for alkali germanate glasses, where an increase of N_{GeO} was used to explain the anomalous behaviour of several

properties [2]. Ge K-edge extended x-ray absorption fine structure (EXAFS) [3, 4] and anomalous x-ray scattering (AXS) [4–6] methods were used to determine Ge–O distances and coordination numbers in GeO_2–P_2O_5 glasses. Experiments on $x GeO_2$–$(1-x)P_2O_5$ glasses, where $0.75 \leqslant x \leqslant 1$, indicate an increase of N_{GeO} from 4.0 to 5.6, and an increase in r_{GeO} distances, from ∼0.175 to ∼180 nm, with increasing P_2O_5 content. Germanophosphate crystal structures [7, 8] show the existence of sixfold coordinated germanium ($^{[6]}$Ge) and so the possibility exists for the formation of a germanophosphate glass network based on PO_4 and GeO_4 tetrahedra and GeO_6 octahedra.

The aim of the present work is to investigate the structure of GeO_2–P_2O_5 glasses through the use of neutron and x-ray diffraction experiments of high resolving power. Such experiments are possible at neutron spallation sources and at synchrotrons supplying hard x-rays. The resolving power of the AXS experiments in [4–6] was not sufficient to obtain all details of the separate P–O and Ge–O peaks. The focus of the present experiments is the better resolution of the P–O and Ge–O peaks and the determination of the parameters of the corresponding distances with high accuracy. Precise N_{GeO} values are needed for discussion of the underlying structural processes responsible for the coordination changes.

For the alkali germanate (A_2O–GeO_2) glasses, the absence of non-bridging oxygens (O_{NB}) indicated that the Ge–O coordination numbers must increase in accordance with the amount of the oxygen introduced by A_2O [9]. Thus, all oxygen atoms should occupy bridging positions (O_B). Diffraction experiments of high resolving power performed on alkali germanate glasses [10, 11] confirmed the increase of N_{GeO} with the additions of A_2O. Analysis of the Ge–O peaks in these studies indicated a fraction of Ge–O distances of ∼0.188 nm which are typical of $^{[6]}$Ge sites [10, 11].

The addition of P_2O_5, a network-forming oxide, is expected to have different effects on the germanate network than would the addition of network-modifying alkali oxides. The structure of glassy (v-)P_2O_5 is formed from PO_4 tetrahedra connected with each other through three corners. The fourth and free corner is occupied by a doubly bonded oxygen (O_{DB}) which is needed to complete the countercharge for compensation of the valency of the P atom [12]. When modifying oxides are added to P_2O_5 glass, the phosphate network disintegrates as non-bridging oxygens form [13, 14] and the 'free corners' of the PO_4 units occupied with O_{DB} participate in the coordination of the modifying cations [14, 15]. The network disintegration ends in the formation of isolated PO_4 units which are connected through four corners to modifying cations.

When a network-forming oxide, such as GeO_2, is added to P_2O_5, new bridging oxygens are shared by both polyhedra, and isolated PO_4 units can be formed which are connected through four corners to the new network-forming cations. One consequence is that the mean coordination number of the 'modifying' species increases. Such behaviour is seen for TeO_2–P_2O_5 glasses [16] where TeO_2 is known as a conditional glass former, i.e., the pure component TeO_2 is difficult to obtain in glassy form. The earlier analyses of the structure of GeO_2–P_2O_5 glasses [3–5] indicate an equivalent increase of N_{GeO}. However, more precise N_{GeO} numbers are needed to confirm the predicted effect of the P_2O_5 added to the glassy germanate networks.

2. Experimental details

Three samples from the GeO_2–P_2O_5 system were prepared with batch compositions of 95, 85 and 75 mol% GeO_2. The glasses were prepared from GeO_2 and $NH_4H_2PO_4$. Measured amounts of each starting material were ground together in a mortar and pestle, placed into

alumina crucibles, and then calcined at 800 °C for 1.5 h to remove ammonia and water from the system. The samples were then melted at temperatures between 1250 and 1400 °C for 30 min before being quenched between copper plates. Compositions were analysed by taking the average of five points using energy dispersive spectroscopy (EDS), which revealed some P_2O_5 loss. The samples are free of significant Al_2O_3 contaminations (all less than 1 mol%). The three samples have 98, 88 and 81 mol% GeO_2, and are labelled gep98, gep88 and gep81, respectively. The densities of the glasses were measured using Archimedes' method with kerosene as the immersion liquid. Measurements were performed on four individual samples of each composition, yielding average densities of 3.587 ± 0.005, 3.577 ± 0.005 and 3.551 ± 0.005 g cm^{-3} for the three glasses, with increasing P_2O_5 content. These values convert to atom number densities of 63.1, 68.7 and 72.0 nm^{-3}, respectively.

The neutron diffraction experiments were performed at the GEM diffractometer [17] of the spallation source ISIS of the Rutherford Appleton Laboratory (Chilton, UK). The glassy material was crushed and loaded into vanadium cylinders 5.0 mm in diameter and with wall thickness of only 0.025 mm. The beam size was 12×40 mm^2. The duration of the data collection was 5 h for gep98 and >10 h for gep88 and gep81. A 6 mm vanadium rod was used to obtain the incident energy spectrum which is needed for data normalization in the time-of-flight regime. The diffraction data were corrected using standard procedures for container and background scattering, attenuation, multiple scattering and inelasticity effects [18]. The differential scattering cross-sections, $d\sigma/d\Omega$, collected in detector groups 2 (13°–21°), 3 (24°–45°), 4 (50°–74°), and 5 (79°–106°) were used to compose the final Faber–Ziman structure factors $S_N(Q)$ [19]. Here Q is the momentum transfer with $Q = (4\pi/\lambda)\sin\theta$; λ is the radiation wavelength and 2θ is the scattering angle. At first, the data of group 5 were normalized to the total scattering cross-section $\sigma/4\pi$. Subsequently, the data of groups 2, 3, 4 were adjusted to those of group 5. After performing a rough Gaussian fitting of the first-neighbour peaks, the normalization was repeated until agreement of the experimental scattering data with model structure factors calculated with parameters of the Gaussian functions was achieved. Figure 1 shows the weighted experimental $Q[S(Q) - 1]$ data and the corresponding model functions.

The x-ray diffraction experiments were performed at the BW5 wiggler beamline at the synchrotron DORIS III of Deutsches Elektronen-Synchrotron (Hamburg). An incident photon energy of 122.5 keV ($\lambda = 0.0101$ nm) was chosen for the experiments. The beam size was 1×4 mm^2. Exact absorption corrections are difficult because the 2.5 mm diameter of the silica capillaries (with wall thickness of 0.01 mm) containing the glassy powder exceeds the beam width. The scattering angles are small ($2\theta = 28°$ for $Q_{max} = 300$ nm^{-1}) and the transmission coefficients are greater than 0.9, and so the absorption is independent of the angle θ. The electronic energy window of the solid-state Ge-detector was chosen to pass the elastic line and the full Compton peak but not fluorescence radiation. The duration of data collection per sample was 8 h. Dead-time corrections were made with a parameter $\tau = 1.08$ μs [20] and a fraction of 0.91 of incident photons is polarized horizontally. Corrections were made for background, container scattering, polarization and absorption. Subsequently, scattering intensities were normalized to the structure-independent scattering functions which were obtained from the tabulated atomic elastic scattering factors [21] and atomic Compton scattering data [22]. Empirical corrections were used in the range $Q > \sim 220$ nm^{-1} to make the scattering intensity oscillate around the structure-independent scattering. Deficits in the calculation of the Compton fraction, uncertainties with the chemical compositions, errors in the instrument calibration, instabilities of beam position and fluctuations of monitor efficiencies can cause the deviations. Finally, the Faber–Ziman structure factors, $S_X(Q)$, are calculated [19, 23].

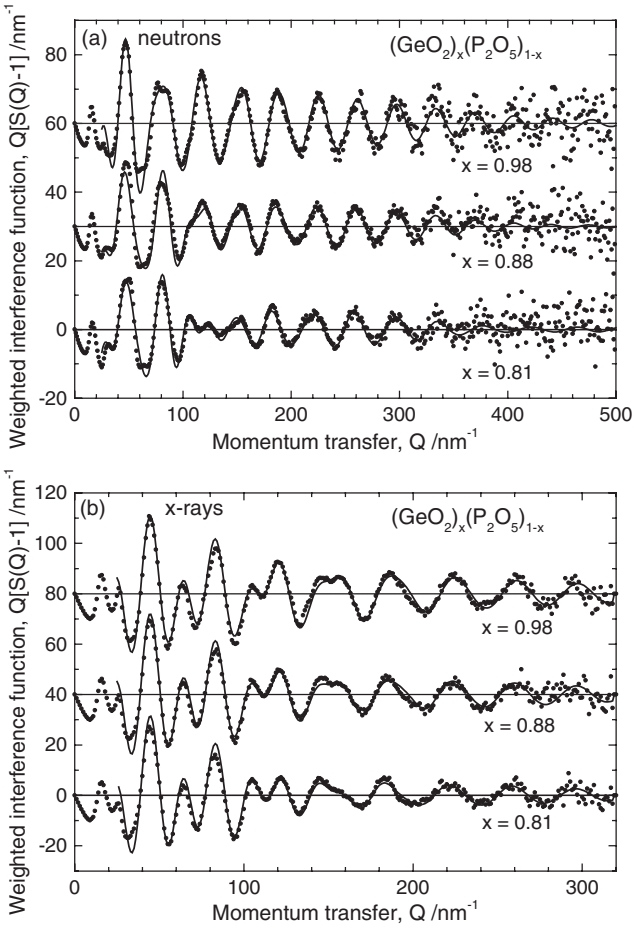

Figure 1. Weighted interference functions of the three samples studied: (a) neutron data and (b) x-ray data. The experimental data (dots) are compared with model functions (lines) which are calculated with the parameters of peaks used for the model $T(r)$ functions shown in figures 2 and 3. Upper functions are shifted for clarity.

3. Results

3.1. Structure factors and correlation functions

The neutron and x-ray structure factors shown in figures 1(a) and (b) are weighted with Q to make visible the oscillations in the high-Q range. The neutron data for $Q > 360$ nm^{-1} are scattered and the corresponding model $Q[S(Q) - 1]$ functions of the samples gep88 and gep81 are very flat in this range. An increase in the data acquisition time would provide limited improvement on the resolution in this region. The x-ray data of gep88 show unphysical differences with the model function at Q of $\sim$280 nm^{-1}.

Since the data of high Q-values are noisy, Fourier transformations (FTs) are performed with damping of $S(Q)$ using $Q_{\max}$ of 500 and 318 nm^{-1} for neutrons and x-rays, respectively. The real-space correlation functions, $T(r)$, are obtained with

$$T(r) = 4\pi r\rho_0 + 2/\pi \int_0^{Q_{\max}} Q[S(Q) - 1]\, M(Q)\, \sin(Qr)\, \mathrm{d}Q \qquad (1)$$

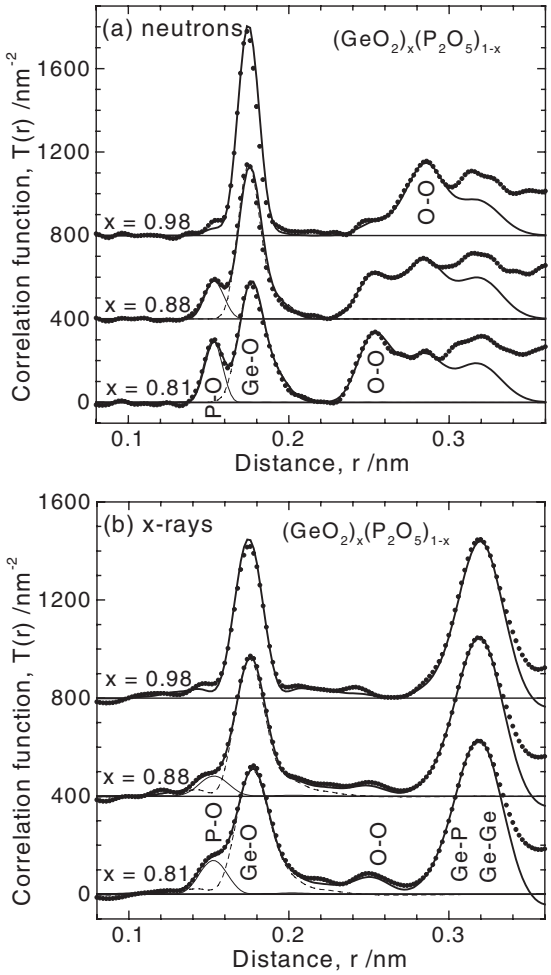

Figure 2. Correlation functions in the range of the first-neighbour peaks of the GeO_2–P_2O_5 glasses (dotted lines): (a) neutron and (b) x-ray data obtained with damping in FT and Q_{max} of 500 and 318 nm^{-1}. The model $T(r)$ functions are given as thick solid lines for which reasonable parameters for the O–O, Ge–P and Ge–Ge peaks are chosen arbitrarily without fits. The model P–O (thin solid lines) and Ge–O (dashed lines) components obtained by peak fitting are shown as separate peaks. Upper functions are shifted for clarity.

where ρ_0 is the number density of atoms and the damping function $M(Q)$ used is $M(Q) = \sin(\pi Q/Q_{max})/(\pi Q/Q_{max})$ [24]. The resulting $T(r)$ functions are shown in figure 2. Since the data ranges with high Q-values are very important for resolving the details of the narrow peaks of covalent bonds, the FT procedures are also repeated without damping and with Q_{max} values of 360 and 318 nm^{-1} for the neutron and x-ray data, respectively. The corresponding $T(r)$ functions without damping are shown in figure 3. The P–O and Ge–O first-neighbour distances are resolved for gep88 and gep81, and are better without damping as shown in figure 3. The fraction of P_2O_5 in gep98 is too small to show significant P–O correlations. The $T(r)$ functions of gep81 plotted in figure 3 (no damping) show clear shoulders at ~0.195 nm which could be interpreted as the contributions from GeO_6 octahedra possessing

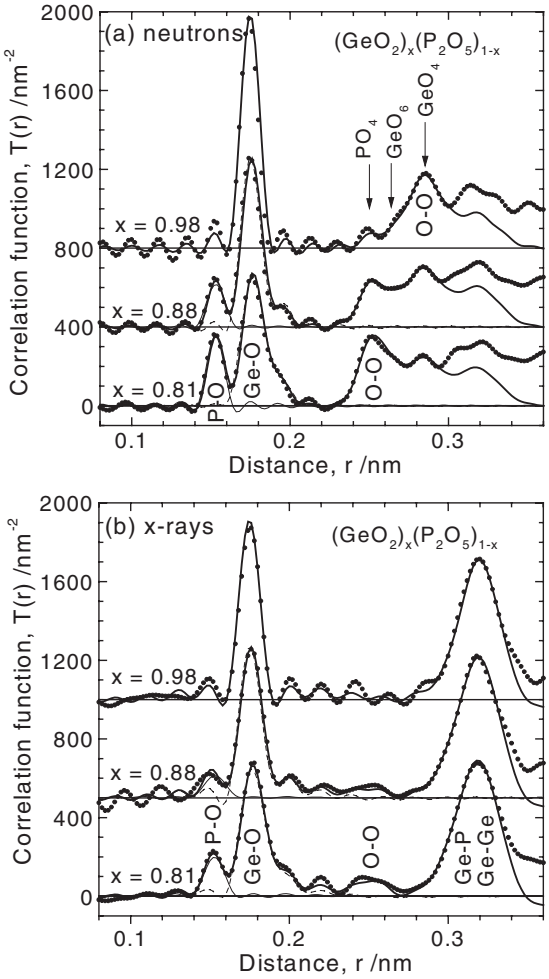

Figure 3. Correlation functions in the range of the first-neighbour peaks of the GeO_2–P_2O_5 glasses (dotted lines): (a) neutron and (b) x-ray data obtained without damping in FT and Q_{max} of 360 and 318 nm^{-1}. The model $T(r)$ functions calculated with the peak parameters already used in figure 2 are given as thick solid lines. The model P–O (thin solid lines) and Ge–O (dashed lines) components are also shown separately. Definite O–O distances are marked by arrows and are related to edge lengths of the structural groups indicated in the plot. Upper functions are shifted for clarity.

greater Ge–O distances; however, peaks at this distance are also found for the other two samples. The peaks are due to satellite ripples caused by the termination effects from FTs according to equation (1) and the shoulder of the Ge–O peak of gep81 appears enhanced from the termination effect. Therefore, the P–O and Ge–O peaks shown in figure 2 exhibit more realistic shapes without the FT termination ripples but the damping causes some peak broadening. The position of the Ge–O peak shifts by 0.002 nm to greater distances in the series gep98 < gep88 < gep81. In addition, there is an increasing asymmetry of the peaks for gep88 and gep81, whereas the peak of gep98 is still nearly symmetric. A separate component at ∼0.188 nm, which could be directly related to [6]Ge sites, is not found in the Ge–O peaks.

Table 1. Parameters resulting from Gaussian fitting of the P–O and Ge–O first-neighbour peaks of the three GeO_2–P_2O_5 glasses. Numbers in parentheses give the uncertainty in the last digit. The parameters of the O–O peak are fixed for all samples.

Sample label	Atom pair	Peak parameters			Ge–O coordination number	Mean Ge–O distance (nm)
		N_{ij}	r_{ij} (nm)	Δr_{ij} (nm)		
gep98	P–O	4.00[a]	0.153[a]	0.010[a]		
	Ge–O	3.65	0.1742	0.011	4.00(20)	0.175(1)
		0.35	0.188	0.020[a]		
	O–O	0.50[a]	0.252[a]	0.020[a]		
		0.50[a]	0.265[a]	0.025[a]		
		5.00[a]	0.285[a]	0.025[a]		
gep88	P–O	4.3(5)	0.153(2)	0.011(2)		
	Ge–O	3.28	0.1747	0.012	4.28(20)	0.178(1)
		1.00	0.188	0.024		
	O–O	1.70[a]	0.251[a]	0.019[a]		
		1.20[a]	0.265[a]	0.025[a]		
		1.60[a]	0.285[a]	0.025[a]		
gep81	P–O	4.14(20)	0.153(1)	0.009(2)		
	Ge–O	3.07	0.1755	0.014	4.51(20)	0.180(1)
		1.44	0.188	0.021		
	O–O	2.40[a]	0.251[a]	0.019[a]		
		2.00[a]	0.265[a]	0.025[a]		
		2.30[a]	0.286[a]	0.022[a]		

[a] These values have been fixed in the fits.

3.2. Gaussian fitting of the first-neighbour peaks

The height of the P–O peak at a bond length of ∼0.155 nm grows continuously with P_2O_5 content. P–O–P bridges are not expected for the glasses with P_2O_5 content less than about 25 mol% [13, 14]. A variety of lengths of P–O bonds in P–O–Ge bridges can arise from links with the different GeO_4, GeO_5 and GeO_6 units. Nevertheless, the fit of the P–O peak is successful with a single Gaussian function. In the case of gep98, the parameters of the model P–O peak are fixed because the peak area is very small. The Ge–O peak at ∼0.175 nm is accompanied by a tail extending to 0.21 nm (figures 2 and 3). Two Gaussian functions are used to fit the Ge–O peak to account for this asymmetry. The parameters of the Gaussian functions are the coordination numbers, N_{ij}, the mean distances, r_{ij}, and the peak widths (full widths at half maximum), Δr_{ij}, for the pairs of atomic species i and j. Gaussian fitting is performed to the $T_N(r)$ and $T_X(r)$ data simultaneously. The effects of termination of the FT integral at $Q_{\max}$ are taken into account by convolution of the Gaussian peaks with functions $P_{ij}(r)$ [25, 26]. This procedure simulates the Q-window and damping used in equation (1). In case of x-ray scattering, different dependences on Q of the weighting factors $w_{ij}(Q)$ cause specific features. For example, flat tails occur on both sides of the Ge–O peaks, extending to 0.13 nm or to 0.24 nm. These effects are reproduced in the model functions by appropriate use of the convolution method mentioned above. Least-squares fits using the Marquardt algorithm [27] are only performed on the $T(r)$ functions obtained with damping (figure 2). Small differences at ∼0.195 nm exist for the model functions of gep88 and gep81 shown in figure 2(a). The resulting peak parameters are listed in table 1. Subsequently, for the $T(r)$ data obtained without damping (figure 3), model functions are calculated by use of these parameters. Here, good agreement is found with even the termination ripples well reproduced. Only in the case of the

x-ray data of gep88 do some differences exist at lengths of ∼0.12 nm. These differences may be caused by the unphysical features at ∼280 nm^{-1} observed in the $Q[S(Q) - 1]$ function of gep88 (figure 1(b)).

The total Ge–O coordination numbers and the corresponding mean distances given in table 1 indicate the formation of $^{[5]}$Ge or $^{[6]}$Ge sites as the P_2O_5 content is increased. The P–O coordination number obtained for all samples are four, within the limits of error. The P–O peaks are narrow and well fitted with a single Gaussian function, as was found for the P–O peaks obtained for TeO_2–P_2O_5 glasses [16].

Some peaks of the O–O, Ge–P, and Ge–Ge correlations are added to the model functions using reasonable peak parameters which are empirically optimized. For example, the O–O peak at ∼0.251 nm, caused by the edges of PO_4 tetrahedra, is needed to correctly simulate the right flank of the Ge–O peak. This O–O contribution increases with increasing P_2O_5 content, whereas that at ∼0.285 nm decreases. The latter distance is due to the edges of the GeO_4 tetrahedra (see figure 3(a)). As P_2O_5 is added, the height of the peak at 0.285 nm decreases to less than that of the peak at 0.251 nm although the number of Ge atoms is still greater than that of P atoms. This fact is a further indication for a change in the coordination of the GeO_4 units. With increasing P_2O_5 content, additional O–O distances occur at ∼0.265 nm. Such lengths can be attributed to the edges of GeO_6 octahedra. In principle, a quantitative analysis of the O–O correlations of the neutron $T(r)$ function could help to determine the fractions of the different GeO_n groups, but the edge lengths of possible GeO_5 polyhedra are not known. Secondly, we do not know the widths of the overlapping O–O correlations of the PO_4 units and the different GeO_n polyhedra. The edge lengths and peak widths of these correlations can change with glass composition. In the x-ray $T(r)$ functions the O–O correlations possess little weight but the Ge–P and Ge–Ge correlations dominate. The P–P peak caused by P–O–P links would appear at ∼0.295 nm, but indications for such linkages in significant numbers are not found.

4. Discussion

4.1. Compositional dependence of the Ge–O coordination number

The Ge–O coordination numbers for the $x GeO_2$–$(1 - x)P_2O_5$ glasses obtained in two independent diffraction experiments possess greater accuracy than the N_{GeO} numbers obtained by AXS [4–6]. The continuous change of N_{GeO}, from 4.0 ± 0.2 to 4.3 ± 0.2 and 4.5 ± 0.2, with decreasing x, is small but significant. These numbers can be compared with the behaviour predicted in section 1, where isolated PO_4 units which are connected through four corners provide additional oxygens to form P–O–Ge bridges to GeO_n units with $n > 4$. The corresponding structural changes are expressed for GeO_5 units by the relationship [16]

$$PO_{3/2}O + GeO_{4/2} \rightarrow (PO_{4/2})^{+} + (GeO_{5/2})^{-} \tag{2}$$

where $O_{1/2}$ represents a bridging oxygen atom (P–O–P, Ge–O–Ge, or Ge–O–P). Some $GeO_{4/2}$ units of v-GeO_2 are converted to Ge units with greater coordination numbers (N_{GeO}) and these new germanate sites are charge-balanced by the formation of isolated $PO_{4/2}$ units from P_2O_5.

Figure 4 shows the dependence of N_{GeO} on composition for the P_2O_5-containing glasses and for Na_2O- and K_2O-containing germanate glasses [10, 11]. The glass compositions are represented by the mole fractions $c(M_zO)$ for the M_aO_b oxides, where $z = a/b$. From equation (2), the effect of composition on N_{GeO} is described by

$$N_{GeO} = 4 + 0.4c(P_{0.4}O)/[1 - c(P_{0.4}O)]. \tag{3}$$

Equation (3) is represented by the dotted line labelled 'model D' in figure 4, as described in an earlier study of the structures of $x TeO_2$–$(1 - x)P_2O_5$ glasses [16]. The present

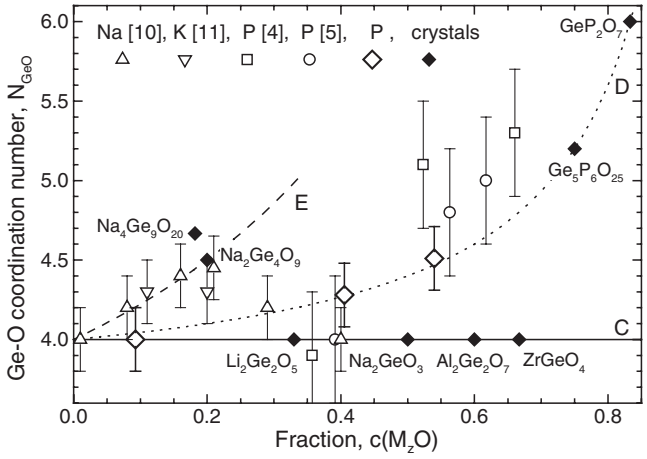

Figure 4. Compositional behaviour of the Ge–O coordination numbers of the GeO_2–P_2O_5 glasses studied, of N_{GeO} values obtained by AXS [4, 5] and of N_{GeO} values of alkali germanate glasses with Na_2O [10] and K_2O [11] versus content of the second component. The N_{GeO} numbers are compared with those of some related crystal structures ($Ge_5O(PO_4)_6$ [7], GeP_2O_7 [8], $Na_4Ge_9O_{20}$ [30], $Na_2Ge_4O_9$ [34], $Li_2Ge_2O_5$ [35], Li_2GeO_3 [36], $Al_2Ge_2O_7$ [31], $ZrGeO_4$ [32]). The dashed, dotted and solid lines specify the behaviour of N_{GeO} according to three compositional models (C, D, and E, respectively) originally developed to understand the N_{TeO} behaviour in binary tellurite glasses [16]. The models are described in the text.

N_{GeO} results match the predicted behaviour very well. The N_{GeO} of two germanophosphate crystal structures [7, 8], where all oxygen atoms are in bridging positions, are found on the corresponding 'model D' line, as well. The AXS results [4–6] follow the 'model D' predictions only roughly. Structural deviations from 'model D' might be due, for example, to some O atoms that have three Ge neighbours (for example as in the rutile form of GeO_2 [29] or in $Na_4Ge_9O_{20}$ [30]), giving a value of N_{GeO} greater than predicted. In germanate crystals with second oxides such as the conditional glass formers Al_2O_3 or ZrO_2 [31, 32], the Ge atoms form only GeO_4 tetrahedra. Glasses of the GeO_2–TeO_2 system have been studied by EXAFS, where the formation of some GeO_6 octahedra was reported [33].

An increase of N_{GeO} is well known for the alkali germanates. Figure 4 shows the N_{GeO} of four crystal structures. The first of them ($Na_4Ge_9O_{20}$ [30]) possesses some oxygens with three $^{[6]}$Ge neighbours. The N_{GeO} values of A_2O–GeO_2 glasses obtained by neutron diffraction of high resolving power [10, 11] are comparable to those indicated by the other three crystal structures [34–36]. Up to compositions with $c(A_2O) \sim 0.2$, all oxygens form Ge–O–Ge bridges, as noted in section 1. The structural changes have been summarized by [37]

$$A_2O + GeO_{4/2} \rightarrow 2A^+ + (GeO_{6/2})^{2-} \tag{4}$$

and the corresponding increase of N_{GeO} is given by 'model E' with

$$N_{GeO} = 4 + 2c(A_2O)/[1 - c(A_2O)]. \tag{5}$$

The octahedral GeO_6 units result from sp^3d^2 hybridization and figure 5(a) shows a representation of their bonding environment. The N_{GeO} of the alkali germanate glasses follows compositional 'model E' up to modifier additions of ~0.2. With additional modifier, the germanate structure returns to that based on GeO_4 units and the formation of non-bridging oxygens becomes significant. A corresponding maximum limit in N_{GeO} is not indicated for the GeO_2–P_2O_5 glasses studied to date [4, 5, this work] or for the related crystals [7, 8].

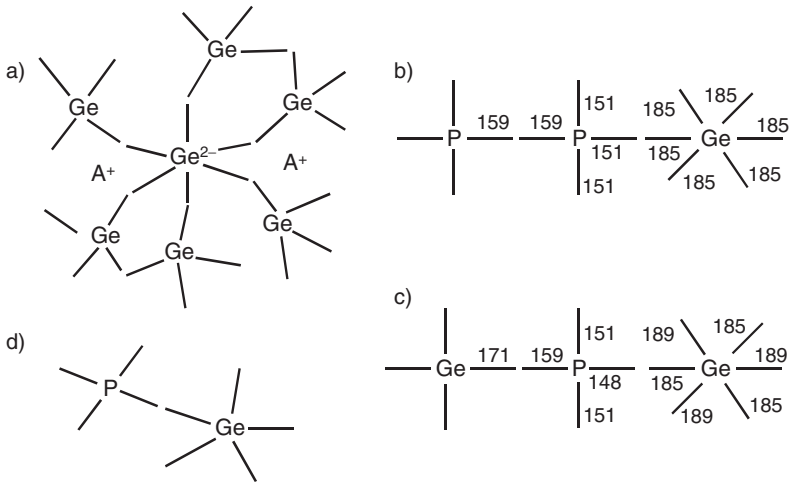

Figure 5. Schemes of germanate networks: (a) linkages to a GeO_6 octahedron in an alkali germanate; (b) linkages between P and Ge units in the GeP_2O_7 crystal [8]; (c) linkages between P and Ge units in the $Ge_5O(PO_4)_6$ crystal [7]; (d) possible linkages between P and Ge units in a structure with 33 mol% P_2O_5. The numbers indicated in the plots are bond lengths given in picometres. Oxygen atoms have been removed for clarity.

The effect of composition on N_{GeO} for the GeO_2–P_2O_5 glasses is similar to that found for the compositional dependences of N_{TeO} for TeO_2–P_2O_5 glasses [16]. In both cases, the reasons for these changes are attributable to properties of the PO_4 units [13–15]. In contrast, when alkali oxides are added to the germanate and tellurite networks, the N_{GeO} and N_{TeO} values have different compositional dependences, as expressed by 'model E' for the germanates and 'model A' (see [16]) for the tellurites. In 'model A', the addition of A_2O reduces N_{TeO} as TeO_4 units are replaced by TeO_3 units.

For alkali additions to GeO_2, the increase of N_{GeO} avoids formation of O_{NB} by forming suitable anionic O_B sites for more uniform distributions of the negative charge needed to balance nearby A^+ ions. In tellurite glasses, alkali additions create O_{NB} such as in silicate networks, but the number of O_{NB} is doubled by the $TeO_4 \rightarrow TeO_3$ transition, which increases the number of suitable O_{NB} sites for more uniform distributions of the negative charge needed to charge balance neighbouring A^+ ions. In the case of the P_2O_5 additions, the N_{GeO} (or N_{TeO}) increases and the formation of isolated $PO_{4/2}$ tetrahedra (equation (2)) with equivalent linkages through their four corners to GeO_n (or TeO_n) units becomes possible.

4.2. Distributions of the P–O and Ge–O bond lengths

The compositional dependence of N_{GeO} discussed above is a direct result from the experimental data. Equation (2) gives an explanation of this dependence based on the $GeO_4 \rightarrow GeO_5$ transition. An analogous relationship could be given for the formation of GeO_6 units, but direct knowledge of the preference for either the $^{[6]}$Ge or $^{[5]}$Ge sites is not available. Clarification is also desired for details of the linkages between the different groups. The P and $^{[5]}$Ge (and/or $^{[6]}$Ge) sites are neighbours through P–O–Ge linkages for reasons of charge balance, but each of the P and $^{[5]}$Ge (and/or $^{[6]}$Ge) sites should also have GeO_4 neighbours because the greatest fraction of Ge in these glasses is tetrahedral.

The distributions of bonds in the structures of the $Ge_5O(PO_4)_6$ [7] and GeP_2O_7 [8] crystals show that the PO_4 tetrahedra possess three $^{[6]}$Ge neighbours but also a $^{[4]}$Ge or P neighbour,

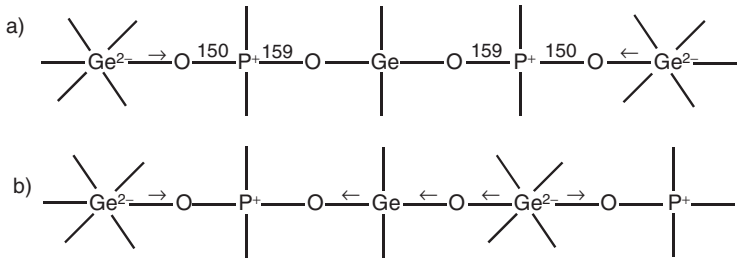

Figure 6. Network sections showing the linkages between the PO_4, GeO_6, and GeO_4 groups (a) as arranged in the $Ge_5O(PO_4)_6$ crystal [7]; (b) as suggested for glasses with P_2O_5 content less than 20 mol%. Arrows indicate the directions of partial shifts of electron charges.

respectively (see figures 5(b) and (c)). The bond lengths in the PO_4 units are different for linkages with octahedra or tetrahedra while the $^{[6]}$Ge form regular octahedra. A structure based on only PO_4 and GeO_5 units (figure 5(d)) is possible (33 mol% P_2O_5), where the P–O bonds of the PO_4 are in equivalent linkages with four $^{[5]}$Ge. GeO_5 polyhedra possess less regular shapes with geometries ranging from square pyramids to trigonal bipyramids; however, uniform environments with equal groups in the neighbouring positions are probably rare for the PO_4 or GeO_n units existing in the structures of the glasses examined here.

The P–O peaks of samples gep88 and gep81 have been approximated with single Gaussian functions. The peak widths are similar to those obtained earlier [28, 38] for either the peaks of the P–O_T or P–O_B bonds. The terminal oxygens (O_T) include the O_{DB} known from the $PO_{3/2}O$ units and the O_{NB} created by breakage of P–O–P bridges using the oxygen of the modifier oxide. The O_{DB} and O_{NB} cannot be differentiated in the PO_4 tetrahedra [14]. The position of the P–O peak at ∼0.153 nm (table 1) is similar to the mean bond lengths found for other binary phosphate glasses [28, 38].

The 'isolated' PO_4 tetrahedra in the crystal structure of $Ge_5O(PO_4)_6$ [7] (figure 5(c)) have different P–O bond lengths in bridges with the $^{[6]}$Ge and $^{[4]}$Ge sites, with $r_{PO} \sim 0.150$ and 0.159 nm, respectively. Observation of split P–O peaks, such as those found for the P–O_T and P–O_B bonds of other binary phosphate glasses [28, 38], is not possible with such distance differences and Q_{max} of only 360 nm^{-1}. But such differences of bond lengths would increase the width of the P–O peak significantly. Due to the change of contrast of the P–O and Ge–O correlations in the x-ray and neutron diffraction data (figures 3(a) and (b)) inappropriate separations of the first-neighbour peaks would become visible but the fits were successful with single and narrow P–O peaks.

The structures of the germanophosphate glasses studied here are expected to differ from that of the $Ge_5O(PO_4)_6$ crystal [7], where $^{[4]}$Ge–O–$^{[6]}$Ge bridges do not exist and, consequently, an optimum exchange of charges with the PO_4 tetrahedra is not possible. In the glasses with greater numbers of GeO_4 units coexisting with the P and $^{[5]}$Ge (and/or $^{[6]}$Ge) neighbours, all the latter sites should possess some GeO_4 neighbours and a GeO_4 unit should form linkages with unlike groups, as well. The balance of bonding forces is accompanied with shifts of charges across the different groups which reduces the differences between the lengths of P–O bonds in the P–O–$^{[n]}$Ge linkages with $n = 4, 5, 6$, as shown in figure 6. According to equation (2), two PO_4 tetrahedra provide the GeO_6 unit with two additional electrons. This consideration implies that the single P–O bonds in the bridges with the $^{[6]}$Ge and $^{[4]}$Ge sites should possess lengths close to those known of P–O_B bonds (∼0.160 nm [28, 38]). However, due to the high positive charge at the P^{5+} ion, part of the negative charge formally given to the GeO_6 is held closer to the P^{5+} (figure 6(b)). The Ge–O bonds of the GeO_6 units appear underbonded and the

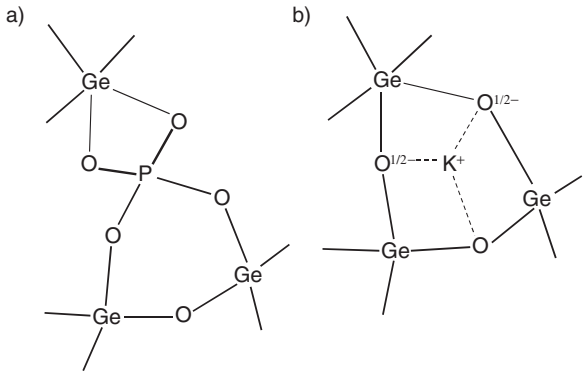

Figure 7. Network sections with (a) PO_4 and, (b) K^+ sites inserted into the germanate structures showing the analogous effect of their incorporation in germanate networks here with adjacent GeO_5 and GeO_4 groups. The P_2O_5 and K_2O contents are less than 0.2. Edge-sharing between the PO_4 and GeO_5 units is only shown for simplicity and is not assumed as a dominating feature.

P–O bonds become overbonded irrespective of the kind of neighbouring GeO_n group. Thus, the small width of the P–O peak should not be used as an indication for links with specific $^{[n]}$Ge. The bonds in the GeO_4 unit behave differently; those in competition with the P sites (P–O–$^{[4]}$Ge linkages) are elongated whereas those in $^{[4]}$Ge–O–$^{[6]}$Ge linkages are shortened.

Despite the differences that exist between the Ge–O coordination change of GeO_2–P_2O_5 and A_2O–GeO_2 glasses, it is worthwhile comparing the Ge–O bond parameters shown in table 1 with the Ge–O parameters reported for K_2O–GeO_2 glasses [11, 39]. An N_{GeO} of ∼4.3 and a mean Ge–O distance of 0.178 nm with the first sharp component at 0.175 nm were found for the K_2O–GeO_2 sample of 11 mol% K_2O [11, 39]; virtually identical structural parameters were obtained for gep88 (table 1). An N_{GeO} of ∼4.3 (neutron data [11]) or ∼4.5 (x-ray data [39]) and a mean distance of 0.180 nm with the first sharp component at 0.1755 nm are reported for the 20 mol% K_2O glass and the same values were obtained for gep81. The first components are more narrow for the K_2O–GeO_2 glasses.

The comparisons of the lengths of the Ge–O bonds and the relationships (2) and (4) indicate that $(PO_{4/2})^+$ groups and K^+ ions will have similar effects on germanate networks (with K_2O fractions less than 20 mol%). Figure 7 shows how both ions can occupy similar sites; in this example, they balance a GeO_5 and two GeO_4 units. The partial shift of negative charge (discussed above) from the $^{[5]}$Ge site to the O atoms leads to underbonded Ge–O bonds in the GeO_5 unit but overbonded P–O bonds (figure 7(a)). Underbonded Ge–O bonds in the GeO_5 unit of the K_2O–GeO_2 glass (figure 7(b)) are balanced by the K^+ ions. The negative charge of the GeO_5 unit is located at those oxygen sites which neighbour the K^+ ions. These two oxygens share the character of an O_B with that of an O_{NB}. This view is overly simple and the exact distribution of charges is more complicated. For example, the third oxygen neighbour of the K^+ ion shown in figure 7(b) should carry more negative charge than that in a simple $^{[4]}$Ge–O–$^{[4]}$Ge bridge. The analogy of K^+ ions and $(PO_{4/2})^+$ groups ends for glasses with K_2O content of ∼20 mol% [10], when non-bridging oxygens form and N_{GeO} decreases to four for K_2O–GeO_2 glasses.

5. Conclusions

The mean Ge–O coordination numbers, N_{GeO}, of GeO_2–P_2O_5 glasses increase with P_2O_5 additions in accordance with the assumption that all oxygen atoms are found in Ge–O–Ge

or P–O–Ge bridges for the glasses studied here, with P_2O_5 content up to 19 mol%. New GeO_6 or GeO_5 polyhedra are formed, coexisting with GeO_4 and isolated PO_4 units, as P_2O_5 is added to the GeO_2 glass. The bond valencies in the P–O bonds are greater than unity and are balanced in P–O–Ge bridges with underbonded Ge–O links from GeO_5 or GeO_6 polyhedra. Mixed site environments are expected for the GeO_5 (or GeO_6) and PO_4 units in glasses with lower P_2O_5 content due to the greater fraction of the GeO_4 tetrahedra. Despite the different groups which are connected to the PO_4 tetrahedra, the peaks of P–O distances are narrow. This behaviour implies that all P–O bonds in the linkages P–O–$^{[n]}$Ge with $n = 4, 5, 6$ are nearly identical and overbonded. The distributions of the first-neighbour Ge–O distances are found to be nearly identical for the GeO_2–P_2O_5 glasses and those reported for K_2O–GeO_2 glasses of equimolar K_2O and P_2O_5 content. This is explained by assuming that the electron as the countercharge of a given K^+ ion is distributed at the adjacent bridging oxygen sites and does not participate in the covalent Ge–O bonds.

Acknowledgments

Financial support of the Deutsche Forschungsgemeinschaft (contract KR 1372/9-1, Rostock University) is gratefully acknowledged, as is the financial support of the National Science Foundation (DMR 0305202, University of Missouri-Rolla).

References

[1] Takahashi K, Mochida N, Matsui H, Takeuchi S and Gohshi Y 1976 *Yogyo-Kyokai-Shi* **84** 482
[2] Ivanov A O and Evstropiev K S 1962 *Dokl. Akad. Nauk SSSR* **145** 797
[3] Shimizugawa Y, Yin C D, Okumo M, Morikawa H, Marumo F, Udagawa Y, Mochida N and Sekiya T 1987 *Yogyo-Kyokai-Shi* **95** 418
[4] Sugiyama K, Waseda Y and Ashizuka M 1991 *Mater. Trans. JIM* **32** 1030
[5] Waseda Y 2002 *Anomalous x-ray Scattering for Materials Characterization: Atomic-Scale Structure Determination* (*Springer Tracts in Modern Physics* vol 179) (Berlin: Springer) pp 125–8
[6] Shimizugawa Y, Marumo F, Nukui A and Ohsumi K 1994 *J. Non-Cryst. Solids* **176** 76
[7] Mayer H and Völlenkle H 1972 *Mh. Chemie* **103** 1560
[8] Kaiser U and Glaum R 1994 *Z. Anorg. Allg. Chemie* **610** 1755
[9] Smets B M J and Lommen T P A 1981 *J. Non-Cryst. Solids* **46** 21
[10] Ueno M, Misawa M and Suzuki K 1983 *Physica* B **120** 347
[11] Hoppe U, Kranold R, Weber H-J and Hannon A C 1999 *J. Non-Cryst. Solids* **248** 1
[12] Wright A C, Hulme R A, Grimley D I, Sinclair R N, Martin S W, Rice D L and Galeener F L 1991 *J. Non-Cryst. Solids* **129** 213
[13] Van Wazer J R 1958 *Phosphorus and Its Compounds* vol 1 (New York: Interscience) p 717 ff
[14] Brow R K 2000 *J. Non-Cryst. Solids* **234/232** 1 and references therein
[15] Hoppe U 1996 *J. Non-Cryst. Solids* **195** 138
[16] Hoppe U, Gugov I, Bürger H, Jóvári P and Hannon A C 2005 *J. Phys.: Condens. Matter* **17** 2365
[17] Hannon A C 2005 *Nucl. Instrum. Methods* A **551** 88
[18] Soper A K and Buchanan P 2004 private communication
Hannon A C 2004 http://www.isis.rl.ac.uk/disordered/Manuals/gudrun/gudrun_GEM.htm
[19] Faber T E and Ziman J M 1965 *Phil. Mag.* **11** 153
[20] Poulsen H F, Neuefeind J, Neumann H-B, Schneider J R and Zeidler M D 1995 *J. Non-Cryst. Solids* **188** 63
[21] Maslen E N, Fox A G and O'Keefe M A 1992 *International Tables for Crystallography* vol C, ed A J C Wilson (Dordrecht: Kluwer) p 476
[22] Hubbell J H, Veigele Wm J, Briggs E A, Brown R T, Cromer D T and Howerton R J 1975 *J. Phys. Chem. Ref. Data* **4** 471
[23] Waseda Y 1980 *The Structure of Non-Crystalline Materials* (New York: McGraw-Hill) p 11
[24] Lorch E A 1969 *J. Phys. C: Solid State Phys.* **2** 229
[25] Mozzi R L and Warren B E 1969 *J. Appl. Crystallogr.* **2** 164
[26] Leadbetter A J and Wright A C 1972 *J. Non-Cryst. Solids* **7** 23

[27] Marquardt D 1963 *SIAM J. Appl. Math.* **11** 431
[28] Hoppe U, Kranold R, Stachel D, Barz A and Hannon A C 2000 *Z. Naturf.* A **55** 369
[29] Baur W H and Khan A A 1971 *Acta Crystallogr.* B **27** 2133
[30] Ingri N and Lundgren G 1963 *Acta Chem. Scand.* **17** 617
[31] Agafonov V, Kahn A, Michel D and Perez y Jorba M 1986 *J. Solid State Chem.* **62** 402
[32] Ennaciri A, Michel D, Perez y Jorba M and Pannetier J 1984 *Mater. Res. Bull.* **19** 793
[33] Osaka A, Qiu J R, Miura Y and Yao J W 1995 *J. Non-Cryst. Solids* **191** 339
[34] Fleet M E and Muthupari S 1998 *J. Solid State Chem.* **140** 175
[35] Völlenkle H and Wittmann A 1968 *Mh. Chemie* **99** 251
[36] Cruickshank D W J, Kálman A and Stephens J S 1978 *Acta Crystallogr.* B **34** 1333
[37] Yiannopoulos Y D, Varsamis C P E and Kamitsos E I 2002 *Chem. Phys. Lett.* **359** 246
[38] Hoppe U, Walter G, Kranold R and Stachel D 2000 *J. Non-Cryst. Solids* **263/264** 29
[39] Hoppe U, Kranold R, Weber H-J, Neuefeind J and Hannon A C 2000 *J. Non-Cryst. Solids* **278** 99